Journal of Power Sources 273 (2015) 495–501

Contents lists available at ScienceDirect

Journal of Power Sources

journal homepage: www.elsevier.com/locate/jpowsour

Differential thermal voltammetry for tracking of degradation in lithium-ion batteries

Billy Wu [a, b, *], Vladimir Yufit [a], Yu Merla [b], Ricardo F. Martinez-Botas [b], Nigel P. Brandon [a], Gregory J. Offer [a, b]

[a] Department of Earth Science and Engineering, Imperial College London, UK
[b] Department of Mechanical Engineering, Imperial College London, UK

HIGHLIGHTS

- A novel method of extracting the same information as slow rate cyclic voltammetry for a lithium-ion battery is presented.
- The method uses galvanostatic operating modes and was shown to be faster than slow rate cyclic voltammetry.
- Experimental and electrochemical modelling proved the technique validity.
- Cycling experiments at elevated temperatures showed the usefulness of the technique in tracking degradation.
- Electrochemical Impedance Spectroscopy measurements tracked the changes in impedance during cycling.

ARTICLE INFO

Article history:
Received 9 July 2014
Received in revised form
4 September 2014
Accepted 19 September 2014
Available online 28 September 2014

Keywords:
Lithium-ion battery
Electrochemical modelling
Battery degradation
Differential thermal voltammetry
Entropy

ABSTRACT

Monitoring of lithium-ion batteries is of critical importance in electric vehicle applications in order to manage the operational condition of the cells. Measurements on a vehicle often involve current, voltage and temperature which enable *in-situ* diagnostic techniques. This paper presents a novel diagnostic technique, termed differential thermal voltammetry, which is capable of monitoring the state of the battery using voltage and temperature measurements in galvanostatic operating modes. This tracks battery degradation through phase transitions, and the resulting entropic heat, occurring in the electrodes. Experiments to monitor battery degradation using the new technique are compared with a pseudo-2D cell model. Results show that the differential thermal voltammetry technique provides information comparable to that of slow rate cyclic voltammetry at shorter timescale and with load conditions easier to replicate in a vehicle.

1. Introduction

Lithium-Ion Batteries (LIB) are the current technology of choice in electric and hybrid vehicle applications due to their high energy and power densities; however, barriers to mainstream adoption include safety and uncertainty in lifetime of these devices. Many degradation modes have been identified in the literature including the growth of the Solid-Electrolyte Interphase (SEI) layer [1,2], lithium-plating [3,4], electrolyte decomposition [5], mechanical fracture of active electrode particles [6,7], cathode dissolution [8] and others [9,10]. The kinetics of these degradation effects are often influenced by the operating conditions. Development of non-destructive diagnostic techniques is therefore required to improve battery lifetime.

Thermodynamically, lithiated carbon anodes such as Meso-Carbon MicroBeads (MCMB), are not stable in most organic carbonate based electrolytes, such as Ethylene Carbonate–Dimethyl Carbonate (EC–DMC) [11]. However, since the SEI layer protects the anode from irreversible reaction with the electrolyte, the formation of a thin, conformal and non-porous SEI on initial cycling is critical to the lifetime and performance of the battery [12]. On the other hand, continual growth of the SEI increases cell resistance and consumes active material leading to power and capacity fade [13].

Measuring capacity loss from galvanostatic charge/discharge curves provides valuable yet limited insight into the underlying physical mechanisms of lithium-ion battery degradation. Many authors have used a reference electrode to decouple anode and cathode processes [5,8,14–16]. However, the integration of a reference electrode is not a trivial task, impractical to implement in an Electric

* Corresponding author. Department of Earth Science and Engineering, Imperial College London, UK.
E-mail address: billy.wu06@imperial.ac.uk (B. Wu).

http://dx.doi.org/10.1016/j.jpowsour.2014.09.127
0378-7753/

Vehicle (EV) and has been reported to affect the cell behaviour [14]. Therefore, a more practical approach is to implement diagnostic techniques that do not necessarily require the use of a reference electrode. These include: Electrochemical Impedance Spectroscopy (EIS) [5,8,17–22], Slow Rate Cyclic Voltammetry (SRCV) [5,8], differential voltage (dV/dQ) [15,16,23–26] analysis, differential capacity (dQ/dV) [19,27–32] analysis and statistical methods [33,34]. Whilst no single technique provides all the required information to decouple physical mechanisms of operation in a whole cell, their use in combination can often provide additional insight.

EIS allows for the decoupling of various resistances in a battery. Authors have made EIS measurements and fitted these parameters to an Equivalent Circuit Model (ECM) in order to try and predict the condition of the battery [20–22]. However, without half-cell measurements or the use of a reference electrode, the large impedances from one electrode can mask lower impedance processes from the other.

Fitting time-domain current/voltage data to equivalent circuits has also been explored as a means of decoupling loss mechanisms. Krishnan et al. [35] developed a non-linear ECM where elements represent physical processes occurring in a battery. By fitting to an ECM, different processes in the battery are decoupled however, since the fitting process is driven by matching simulated voltages to experimental data, cathodic processes can dominate over anodic ones as the potential variation of the cathode is considerably larger than the anode in many battery chemistries.

dV/dQ and dQ/dV analysis are techniques used to measure the stoichiometric alignment of electrodes within a full lithium-ion battery without the need for a reference electrode. Half-cell measurements allow for the assignment of peaks to anodic or cathodic processes. In dV/dQ analysis, the peaks represent phase transitions in the electrodes, whilst in dQ/dV analysis, the peaks represent the location of a phase equilibrium. A drawback of dQ/dV analysis is that, depending on the step size and battery chemistry, dV can tend to zero causing an infinite solution [16], or in the case noisy data, can cause large variations in the results. A drawback of dV/dQ is that the peaks are defined by changes in the overall cell voltage, which is the difference between the anode and cathode potentials. In the majority of battery chemistries, cell voltage is largely determined by the cathode potential meaning that anode processes are more difficult to discern [27].

Bloom et al. [15,16] and Smith et al. [24] analysed the degradation process in lithium-ion cells using dV/dQ curves and showed that the shift in the peak locations can indicate different mechanisms of capacity fade. Here conclusions about the degradation processes occurring were alluded to by fitting the dV/dQ data to half-cell measurements of fresh electrodes. Fathi et al. [23] also demonstrated the use of dV/dQ with other techniques including EIS and coulombic efficiency measurements to probe the degradation processes in Lithium Cobalt Oxide (LCO)–graphite cells.

Examples of dQ/dV being combined with other techniques include Dubarry et al. [27], who presented a combined thermodynamic State-Of-Charge (SOC) and dQ/dV analysis to decouple thermodynamic and kinetic processes. Smith et al. [28] also combined dQ/dV analysis with high precision end-point capacity measurements to differentiate various degradation mechanisms such as SEI growth, electrolyte decomposition and positive electrode capacity loss. This however requires accurate half-cell V–Q data to be taken as a reference data set. Smith and Dahn [29] then proposed comparing dQ/dV curves from cycle-to-cycle (delta dQ/dV) as another metric to allow for quality assurance in seemingly stable cell chemistries with differences seen in the dQ/dV results within a few cycles.

Statistical analysis of data has also been used. For example, Hu et al. [34] demonstrated that the sample entropy taken from the time-series voltage/current data of a cell correlates with the capacity loss and could be used as an SOH estimator. This method however does not provide physical insight into the mechanisms of degradation in lithium-ion batteries.

As most electrochemical methods require isothermal conditions, temperature measurements are often not required. However, the temperature variation during non-isothermal measurement can contain indirect information about thermodynamic phenomena coupled with electrochemical processes. For instance, the Open Circuit Potential (OCP) of an LIB is temperature dependent and this dependency can be utilised to derive thermodynamic information of the electrode [36].

Reynier et al. [36] showed that in well graphitized carbons, entropy changes during a phase transition follows a staging process as the electrode is lithiated. Maher and Yazami [37] later showed that during cycling of an LIB with a graphite anode and LCO cathode, the entropy change of the cell can indicate degradation mechanisms occurring in either the anode or cathode. During cycling experiments, they showed that significant entropy changes occurred at specific SOCs and these were mostly attributed to the cathode ageing.

These changes in the electrode structure and alignment will affect the amount of entropic heat generated during operation and can therefore act as a battery state indicator. It can be seen from the literature that a number of different diagnostic techniques currently exist, however no single technique can adequately provide all the required information to infer the mechanisms of degradation. To this end, researchers are increasingly combining different techniques in order to circumvent some of the disadvantages of each technique. Hereafter, a novel method of determining the phase transitions of battery electrodes through changes in the entropic heat generation under galvanostatic operation is proposed and validated against simulation and test data. This serves as an additional diagnosis tool to supplement other techniques.

2. Lithium-ion battery model

A pseudo-2D thermo-electrochemical model of an LIB was developed based on the governing equations and modelling framework presented in Refs. [38–41] which considers three porous domains: the anode, separator and cathode. Four partial differential equations describe the unsteady concentration profiles of lithium and lithium-ions in the solid and electrolyte phases, respectively, under charge conservation. The reaction current density was then calculated through the Butler–Volmer equation and the system of equations was iteratively solved. This was coupled to a lumped thermal capacitance model as described by Eqs. (1)–(6). For full details of the governing equations and solution method are provided in Wu et al. [40]. Here the effect of entropic heat generation was added.

$$\rho C_p \frac{\partial T}{\partial t} = q_r + q_j + q_c + q_e - q_{\text{conv}} \tag{1}$$

$$q_r = A \int_0^L j^{\text{Li}} (\phi_s - \phi_e - U) \mathrm{d}x \tag{2}$$

$$q_j = A \int_0^L \left[\sigma^{\text{eff}} \left(\frac{\partial \phi_s}{\partial x} \right)^2 + \kappa^{\text{eff}} \left(\frac{\partial \phi_e}{\partial x} \right)^2 + \kappa_D^{\text{eff}} \left(\frac{\partial \ln c_e}{\partial x} \right) \left(\frac{\partial \phi_e}{\partial x} \right) \right] \mathrm{d}x \tag{3}$$

$$q_c = I^2 \frac{R_c}{A} \tag{4}$$

$$q_e = A \int_0^L j^{\mathrm{Li}} T \left(\frac{\partial E_{\mathrm{OCP}}}{\partial T} \right) \quad (5)$$

$$q_{\mathrm{conv}} = hA_s(T - T_{\mathrm{amb}}) \quad (6)$$

Here ρ is the density of the battery, C_p is the specific heat capacity, T is the cell temperature, t is the time, q_r, q_j, q_c, q_e and q_{conv} are the reaction, joule, contact, entropic and convective heat generation/dissipation, A is the total through-plane area of the electrodes, L is the through-plane thickness, j^{Li} is the reaction current density, ϕ_s is the solid phase potential, ϕ_e is the electrolyte potential, E_{OCP} is the OCP of the electrode, σ^{eff} is the effective conductivity of the solid phase, κ^{eff} is the effective conductivity of the electrolyte, κ_D^{eff} is the effective diffusional conductivity of the electrolyte, I is the applied current, R_c is the contact resistance, a is the specific surface area of the electrode, h is the convective heat transfer coefficient, A_s is the external surface area of the cell and T_{amb} is the ambient temperature.

The battery model was parameterised against test data taken from a Maccor 4300 battery tester for a 4.8 Ah Dow Kokam lithium-polymer battery which used a carbon anode with an NMC cathode. Pulse discharge tests in a 4-electrode mode configuration, consisting of a 3.6 A load for 100 s followed by a 900 s rest period, were used to determine the OCP as well as the diffusion coefficients. The OCP was taken as the steady state value after the rest period. Temperature measurements were made with a k-type thermocouple placed at the centre of the outer cell surface with Kapton® tape. A genetic algorithm based subroutine was used to fit the diffusion and charge transfer coefficients to each consecutive pulse as shown in Fig. 1a [42]. The thickness of the electrode layers were determined by the physical dimensions of the cell and x-ray computed tomography scans of a delaminated cell [43] to find the number of layers. Through-plane thickness ratios of the anode-separator-cathode were based on the values given by Smith and Wang [39].

$\partial E_{\mathrm{OCP}}/\partial T$ measurements were carried out using the apparatus presented by Troxler et al. [44]. Whole cell entropy measurements were used to derive the half-cell entropy profiles by subtracting the anode entropy profile, presented by Reynier et al. [36], from the whole cell measurements and electrode stoichiometric ratios presented by Smith and Wang [39], resulting in the profiles as shown in Fig. 1b.

The resulting voltage and temperature response, under galvanostatic discharge, are shown in Fig. 2a and b, respectively. Here the

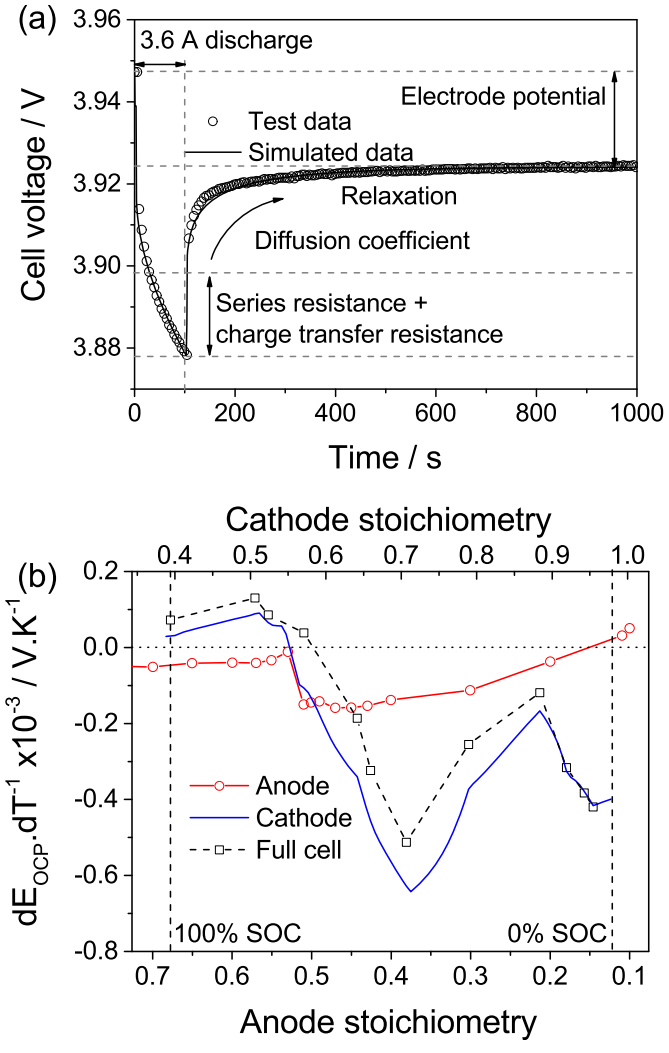

Fig. 1. (a) Pulse discharge of a 4.8 Ah Kokam lithium-polymer cell. (b) Entropy profile for the anode and cathode.

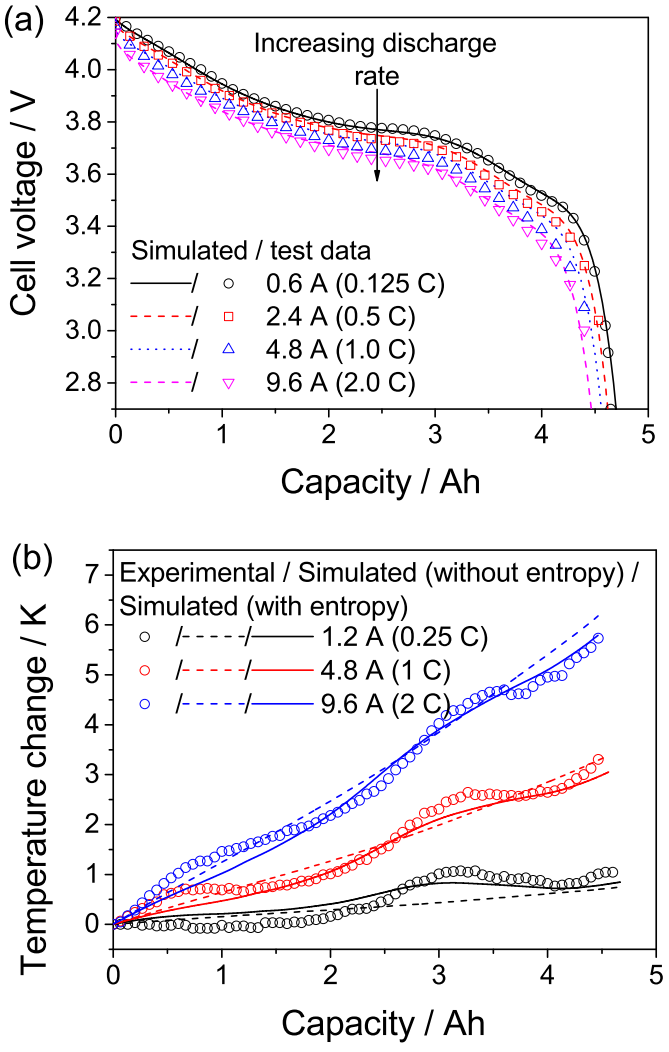

Fig. 2. (a) Comparison of simulation and experimental voltages under galvanostatic discharge. (b) Comparison between simulated and experimental temperatures under discharge.

effect of including and excluding the entropic heats is presented for comparison.

3. Differential thermal voltammetry

SRCV measurements are commonly applied to the study of LIBs, where the current peaks can indicate the onset of a phase transition in the battery electrode. Fig. 3a shows good agreement between the experimental and simulated SRCV profiles for the 4.8 Ah cell at scan rates between 10 and 200 μV s^{-1} during discharge. Slower scan speeds reveal more peaks with the location closer to the true thermodynamic potential due to the lower overpotential contributions.

The disadvantage of SRCV follows from long measurement times (100 μV s^{-1} equates to ~4 h scan time in one direction) and difficulty in the implementation on an EV. We hereafter introduce the concept of Differential Thermal Voltammetry (DTV) as a technique comparable to SRCV but requiring considerably less time through galvanostatic operating modes, which are more common in EV applications.

The DTV technique involves a galvanostatic charge/discharge of a cell with simultaneous measurement of the voltage and temperature. The ratio of the temperature and voltage differentials, with respect to time, are then calculated to give the DTV metric as shown in Eq. (7), where T, V and t represent temperature, voltage and time, respectively.

$$\mathrm{DTV} = \frac{\mathrm{d}T}{\mathrm{d}t} \Big/ \frac{\mathrm{d}V}{\mathrm{d}t} = \frac{\mathrm{d}T}{\mathrm{d}V} \tag{7}$$

During (de)intercalation, the electrodes experience phase transformations which affect the amount of entropic heat generated and the rate of change of the electrode potentials. The decoupled $\partial E_{OCP}/\partial T$ values, as a function of the stoichiometry, for each electrode are shown in Fig. 1b. These changes in the entropic heats can be used as a stoichiometric marker for the respective electrode since this is a function of the SOC. Here it is assumed that the rate of change of the series, SEI and charge transfer resistances, as a function of the SOC, is relatively small, which is a valid assumption, above 3.6 V, when considering the EIS fitted impedance data shown in Fig. 3b. The EIS measurements presented were performed with a Biologic VSP multichannel potentiostat equipped with a 5 A booster under a 1 C (4.8 A) DC load with a 200 mA RMS current oscillation in order to get representative values of the resistance during the DTV measurements. Fitting of equivalent circuit parameters was done with ZView to the equivalent circuit shown in Fig. 3b. Under OCP conditions, the trend in the resistances are the same but the charge transfer resistance is higher as suggested by the Butler–Volmer equation. Therefore, the rate of change of the heat generation is mainly a function of the entropic heat variation with SOC. The rate of change of the voltage also provides information about phase changes occurring in the battery electrodes, with a plateau suggesting a transition. Plotting the DTV metric against the cell voltage thus gives a plot similar to that of SRCV as shown in Fig. 3c which compares the DTV measurement, taken at 2 C, against the 100 and 200 μV s^{-1} SRCV measurements. The dominant peak around 3.65 V appears in both data sets as well as the two smaller peaks at 3.45 V and 4 V. In general, the location of the peaks for the DTV is shifted more to the left due to the higher overpotentials. It should be noted that, in SRCV, the IR-drop is not constant over the voltage window.

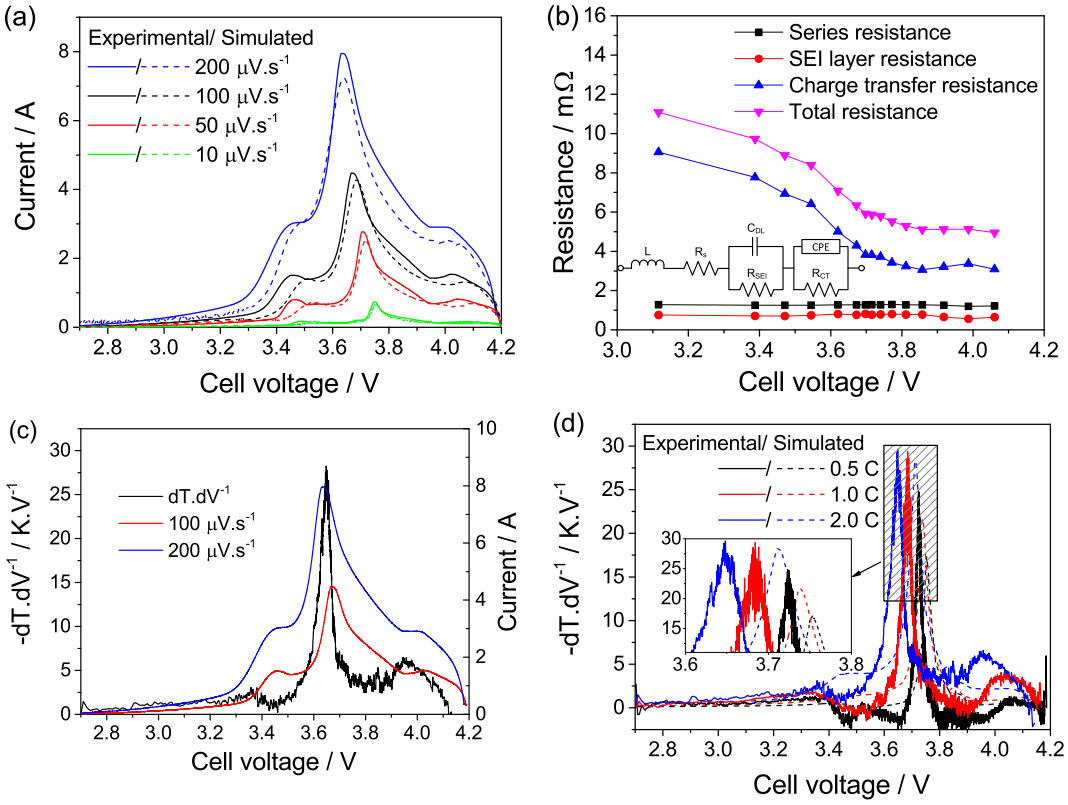

Fig. 3. (a) Simulated and experimental slow rate cyclic voltammetry for a 4.8 Ah lithium-polymer cell for scan rates of 10–200 μV s^{-1}. (b) Equivalent circuit fitted resistance values to EIS measurements at different cell voltages under a 4.8 A DC load with 200 mA RMS excitation current. (c) Comparison between SRCV and DTV measurement made at a 2 C scan rate. (d) Comparison between experimental and simulated DTV for different discharge rates. All measurements and simulations were done at a room temperature.

Discharging at increasing C-rates produces the same information however the IR-drop is higher and therefore the peak position is shifted even more as shown in Fig. 3d, which also corresponds well with the simulated data. The magnitude of the shift in peak location is expected to vary non-linearly due to the non-linear variation of the polarisation resistance with increasing current. The height of the peak is also larger due to the larger entropic heat. The DTV measurements presented were performed under an ambient temperature of 20 °C with natural convection boundary conditions on the cell surface. Provided temperature variations caused by convective heat transfer is minimised over the d*V* measurement range, the influence of thermal boundary conditions on the DTV measurements should be minimal. Under ideal conditions, ambient temperature should be kept constant or the cell should be fully insulated.

4. Degradation tests

To demonstrate the DTV technique, a 4.8 Ah Kokam cell was cycled at 1 C and 55 °C. Thermal conditions were maintained with an Esco Isotherm incubator with a thermal accuracy of ±0.5 °C. During the cycling of the cells, the cathode, anode and electrolyte will degrade however to a different extent. We assume that under this mode of cycling, the SEI layer growth is expected to be the dominant degradation mechanism due to the high temperature operation accelerating the rate of the side reaction associated with the SEI layer growth and electrolyte decomposition [10,13]. After every 50 cycles, the cell was characterised through SRCV, EIS and DTV measurements at room temperature. Fig. 4a shows the SRCV measurements taken at 150 μV s^{-1} at different stages of degradation, and Fig. 4b the percentage of remaining capacity, calculated by

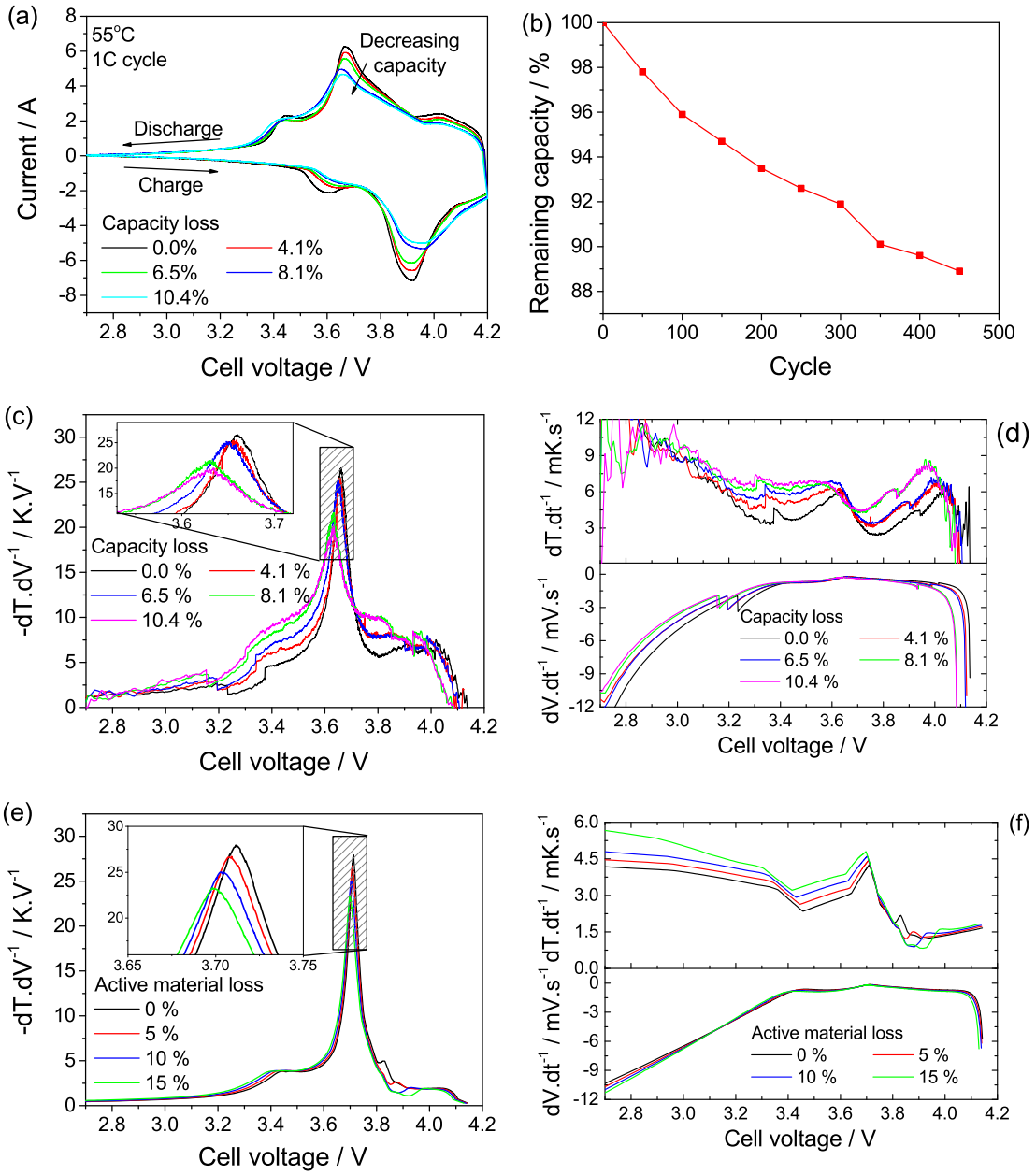

Fig. 4. (a) SRCV measurements taken at 150 μV s^{-1} and room temperature for a cell cycled at 1 C at 55 °C. (b) Relative capacity as a function of number of cycles. (c) DTV measurements taken at 2 C and room temperature for the same cell with decoupled d*T* and d*V* values (d). (e) Simulated DTV measurements with different fractions of material loss with decoupled d*T* and d*V* values (f).

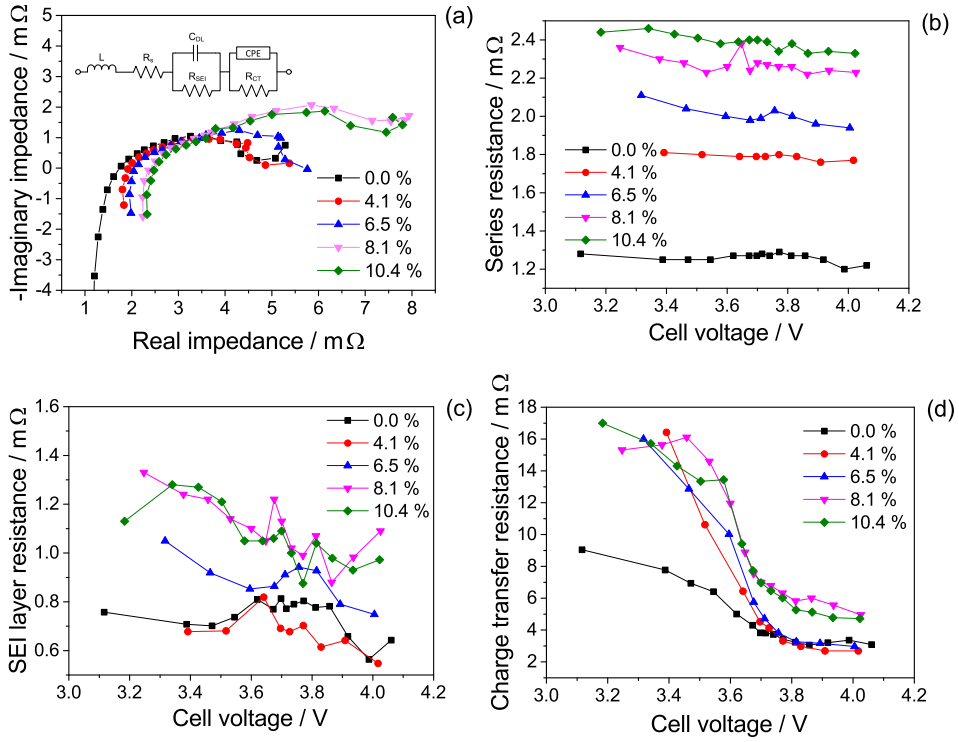

Fig. 5. (a) EIS spectra taken under a 4.8 A DC load at 100% SOC at different capacity loss points with fitted series resistance (b), SEI layer resistance (c) and charge transfer resistance (d) as a function of cell voltage.

integrating the current from the SRCV measurements, as a function of the number of cycles. An increase in total battery resistance caused the main peak to shift and a loss of active material caused a decrease in the area under the curve.

Fig. 4c shows the DTV measurements, with the decoupled $dT \cdot dt^{-1}$ and $dV \cdot dt^{-1}$ values (Fig. 4d), taken at the same corresponding capacity loss points. The same shift to lower potentials in the main peak is observed as in the SRCV, as well as the decrease in peak height. Simulation results of the DTV measurements (Fig. 4e), with the decoupled $dT \cdot dt^{-1}$ and $dV \cdot dt^{-1}$ values (Fig. 4f), where the amount of active material in both the anode and cathode has been reduced, also shows the same trend in the peak position. Here active material is lost from the system in an analogous mechanism to SEI layer growth which is likely to be accelerated during high temperature operation. Discrepancies between the test data and the simulated data still exist since the model does not accounting for all mechanisms of degradation yet.

Fig. 5a–d shows the EIS spectra measured under a 4.8 A load from 1 kHz to 0.1 Hz at 100% SOC for the cell at the different capacity loss points with the fitted parameters for the series, SEI and charge transfer resistances as a function of the cell voltage. Over the operating range, the series resistance remains relatively constant, however with capacity loss there is an upwards trend in increasing resistance. SEI layer and charge transfer resistances also increase with capacity loss suggesting that the main cause of degradation under this mode of operation was associated with increased SEI film resistance on the anode and likely lower electrolyte conductivity due to electrolyte decomposition during SEI formation. Observations in the literature suggest that under 1 C cycling conditions of NMC/graphite based batteries at room temperature, the loss of cycleable lithium was mainly due to lithium consumption during SEI layer growth. The increase in charge transfer resistance was mainly attributed to cathode dissolution processes that catalyse SEI layer growth [5]. It is also probable that cycling of the battery causes microcracks in the electrodes through volume expansion, leading to loss of electrical contact for active material particles and thus an increase in internal resistance of the battery and consequently a reduction in capacity and power.

5. Conclusion

A novel technique, termed the Differential Thermal Voltammetry, has been presented. The DTV technique has been shown to provide equivalent information to SRCV measurements by taking the differential of the measured voltage and temperature during galvanostatic operation. Changes in the entropic heat generation during galvanostatic discharge represent the phase transitions in the battery electrodes. This is typically represented by the current peak when doing SRCV and therefore gives equivalent information. This has the advantage of being faster than SRCV and obtained through galvanostatic operating modes, which are more applicable to EV applications. DTV has therefore been demonstrated as a complimentary tool to existing diagnostic techniques with the novelty of inferring thermodynamic information through temperature measurements. The majority of other techniques rely more on incremental capacity and cell potential variations which, in the majority of battery chemistries, is mostly driven by cathodic processes due to large variations in the half-cell potential of the cathode relative to the anode.

Application of the DTV technique in tracking battery degradation was demonstrated by cycling a 4.8 Ah lithium-polymer cell at elevated temperatures. DTV and SRCV measurements showed that the new technique gives analogous information. EIS measurements suggest that the dominant degradation mechanism at elevated temperature was SEI layer growth, leading to power and capacity fade.

Acknowledgement

The authors would also like to acknowledge the EPSRC for funding of this work, through the Career Acceleration Fellowship for Gregory Offer (EP/I00422X/1) and the EPSRC Funded Energy

Storage for Low Carbon Grids Project (EP/K002252/1) for Billy Wu as well as Climate KIC for Yu Merla.

References

[1] E. Peled, J. Electrochem. Soc. (1979) 2047.
[2] E. Peled, D. Golodnitsky, G. Ardel, J. Electrochem. Soc. 144 (1997) 208.
[3] S. Tippmann, D. Walper, L. Balboa, B. Spier, W.G. Bessler, J. Power Sources 252 (2014) 305.
[4] N. Legrand, B. Knosp, P. Desprez, F. Lapicque, S. Raël, J. Power Sources 245 (2014) 208.
[5] B. Stiaszny, J.C. Ziegler, E.E. Krauß, J.P. Schmidt, E. Ivers-Tiffée, J. Power Sources 251 (2014) 439.
[6] V. Malavé, J.R. Berger, H. Zhu, R.J. Kee, Electrochim. Acta 130 (2014) 707.
[7] C. Lim, B. Yan, L. Yin, L. Zhu, Electrochim. Acta 75 (2012) 279.
[8] B. Stiaszny, J.C. Ziegler, E.E. Krauß, M. Zhang, J.P. Schmidt, E. Ivers-Tiffée, J. Power Sources 258 (2014) 61.
[9] J. Vetter, P. Novák, M.R. Wagner, C. Veit, K.-C. Möller, J.O. Besenhard, M. Winter, M. Wohlfahrt-Mehrens, C. Vogler, A. Hammouche, J. Power Sources 147 (2005) 269.
[10] X. Lin, J. Park, L. Liu, Y. Lee, A.M. Sastry, W. Lu, J. Electrochem. Soc. 160 (2013) A1701.
[11] B. Scrosati, J. Garche, J. Power Sources 195 (2010) 2419.
[12] P. Verma, P. Maire, P. Novák, Electrochim. Acta 55 (2010) 6332.
[13] P. Ramadass, B. Haran, P.M. Gomadam, R. White, B.N. Popov, J. Electrochem. Soc. 151 (2004) A196.
[14] J.P. Christophersen, C.D. Ho, C.G. Motloch, D. Howell, H.L. Hess, J. Electrochem. Soc. 153 (2006) A1406.
[15] I. Bloom, J.P. Christophersen, D.P. Abraham, K.L. Gering, J. Power Sources 157 (2006) 537.
[16] I. Bloom, A.N. Jansen, D.P. Abraham, J. Knuth, S.A. Jones, V.S. Battaglia, G.L. Henriksen, J. Power Sources 139 (2005) 295.
[17] W. Waag, S. Käbitz, D.U. Sauer, Appl. Energy 102 (2013) 885.
[18] U. Troltzsch, O. Kanoun, H. Trankler, Electrochim. Acta 51 (2006) 1664.
[19] Q. Zhang, R.E. White, J. Power Sources 173 (2007) 990.
[20] R.R. Richardson, P.T. Ireland, D.A. Howey, J. Power Sources (2014).
[21] J. Gomez, R. Nelson, E.E. Kalu, M.H. Weatherspoon, J.P. Zheng, J. Power Sources 196 (2011) 4826.
[22] D. Howey, P. Mitcheson, V. Yufit, G. Offer, N. Brandon, IEEE Trans. Veh. Technol. (2014) 1.
[23] R. Fathi, J.C. Burns, D.A. Stevens, H. Ye, C. Hu, G. Jain, E. Scott, C. Schmidt, J.R. Dahn, J. Electrochem. Soc. 161 (2014) A1572.
[24] A.J. Smith, H.M. Dahn, J.C. Burns, J.R. Dahn, J. Electrochem. Soc. 159 (2012) A705.
[25] H.M. Dahn, A.J. Smith, J.C. Burns, D.A. Stevens, J.R. Dahn, J. Electrochem. Soc. 159 (2012) A1405.
[26] J.E. Harlow, D.A. Stevens, J.C. Burns, J.N. Reimers, J.R. Dahn, J. Electrochem. Soc. 160 (2013) A2306.
[27] M. Dubarry, V. Svoboda, R. Hwu, B. Yann Liaw, Electrochem. Solid-State Lett. 9 (2006) A454.
[28] A.J. Smith, J.C. Burns, J.R. Dahn, Electrochem. Solid-State Lett. 14 (2011) A39.
[29] A.J. Smith, J.R. Dahn, J. Electrochem. Soc. 159 (2012) A290.
[30] X. Han, M. Ouyang, L. Lu, J. Li, Y. Zheng, Z. Li, J. Power Sources 251 (2014) 38.
[31] J. Shim, R. Kostecki, T. Richardson, X. Song, K.A. Striebel, 112 (2002) 222.
[32] R. Deshpande, M. Verbrugge, Y.-T. Cheng, J. Wang, P. Liu, J. Electrochem. Soc. 159 (2012) A1730.
[33] E.V. Thomas, I. Bloom, J.P. Christophersen, V.S. Battaglia, J. Power Sources 184 (2008) 312.
[34] X. Hu, S.E. Li, Z. Jia, B. Egardt, Energy 64 (2014) 953.
[35] K.S. Hariharan, V. Senthil Kumar, J. Power Sources 222 (2013) 210.
[36] Y.F. Reynier, R. Yazami, B. Fultz, J. Electrochem. Soc. 151 (2004) A422.
[37] K. Maher, R. Yazami, J. Power Sources 247 (2014) 527.
[38] M. Doyle, J. Newman, J. Electrochem. Soc. 143 (1996) 1890.
[39] K. Smith, C.-Y. Wang, J. Power Sources 160 (2006) 662.
[40] B. Wu, V. Yufit, M. Marinescu, G.J. Offer, R.F. Martinez-Botas, N.P. Brandon, J. Power Sources 243 (2013) 544.
[41] G. Ning, B.N. Popov, J. Electrochem. Soc. 151 (2004) A1584.
[42] B. Wu, Fuel Cell Hybrid Electric Vehicle Powertrain Modelling and Testing (Ph.D. thesis), Imperial College London, 2014.
[43] V. Yufit, P. Shearing, R.W. Hamilton, P.D. Lee, M. Wu, N.P. Brandon, Electrochem. Commun. 13 (2011) 608.
[44] Y. Troxler, B. Wu, M. Marinescu, V. Yufit, Y. Patel, A.J. Marquis, N.P. Brandon, G.J. Offer, J. Power Sources (2013) 1.